Evaporation of the ammonia from the solution described above leaves the solid potassium salts of the two anion radicals and the neutral nitrobenzenes in the reaction apparatus. The neutral nitrobenzenes can be easily distilled from this mixture under high vacuum, leaving only the solid K^+PhNO_2-$^{14}N^{\cdot-}$ and K^+PhNO_2-$^{15}N^{\cdot-}$. Recovery of the isotopically mixed nitrobenzenes is easily accomplished by reacting the solid anion radical salts with iodine dissolved in diethylether. The extra electrons are transferred from the anion radical to the I_2 to form I^- as shown in reaction (2):

$$K^+PhNO_2^{\cdot-} + 1/2I_2 \rightarrow KI + PhNO_2 \quad (2)$$

Because the mixture of solid anion radicals was enriched in $PhNO_2$-$^{15}N^{\cdot-}$ relative to the original mixture of isotopes, the neutral nitrobenzenes remaining after the I_2 addition are similarly enriched in $PhNO_2$-^{15}N. Thus, the addition of a deficient number of electrons to a mixture of isotopically substituted nitrobenzenes, followed by separation of the anions from the remaining neutral species, leaves a ^{15}N-enriched nitrobenzene anion radical. The ^{15}N-enriched neutral species can be recovered by adding iodine to this mixture of anion radical salts. The enriched mixture can be further enriched in ^{15}N by simply subjecting this new mixture repeatedly to the same process. Starting from ordinary nitrobenzene containing 0.37% ^{15}N (natural abundance), it would take 16 passes through this procedure (assuming the efficiency is constant) to produce a sample of 99% pure $PhNO_2$-^{15}N.

The diminished electron affinity of $PhNO_2$-^{14}N relative to that of $PhNO_2$-^{15}N comes from two effects: an electronic effect and a zero-point energy effect. It has been observed that the substitution of a hydrogen by a deuterium in benzene removes the degeneracy of the symmetric and antisymmetric wave functions[4]. Furthermore, alkyl substituents on the benzene anion radical have the same, albeit stronger, effect, and the alkyl substitution leads to a diminished solution electron affinity[5]. Delvin[6] has noted that the presence of an added electron in tetracyanoethylene can alter the zero-point energies of the C-C and C-N stretching modes by as much as 25 cm^{-1}. As the nitrogen atom in nitrobenzene is bound to three other atoms and the spin density on the nitrogen atom in $PhNO_2^{\cdot-}$ is large (the nitrogen coupling constant is 10.2 Gauss), this zero-point energy effect could account for a significant portion of the enhanced electron affinity caused by the replacement of ^{14}N by ^{15}N in nitrobenzene.

We believe that the behaviour we have observed in the isotopically different nitrobenzenes is common for systems where the electron density is large on the isotopically substituted atom. This is supported by the fact that our reductions of mixtures of benzophenone-^{12}C and benzophenone-^{13}C (BZO-^{12}C and BZO-^{13}C) in hexamethylphosphoramide with potassium metal,

$$BZO\text{-}^{12}C^{\cdot-}K^+ + BZO\text{-}^{13}C \rightleftharpoons BZO\text{-}^{12}C + BZO\text{-}^{13}C^{\cdot-}K^+ \quad (3)$$

show that the solution electron affinity of the BZO-^{12}C is significantly greater than that of BZO-^{13}C ($K_{eq} = 0.58 \pm 0.04$ at 10 °C).

The observations reported for both ^{15}N and ^{13}C systems represent an isotope effect on solution electron affinity which is an order of magnitude larger than the usual isotope effects, and is not significantly dependent on the mass ratio, as is usually the case. This suggests the feasibility of isotopic enrichment processes based on partial reduction of mixtures of neutral isotopic species followed by simple physical or chemical separation of the resulting ions from the neutral species in the resulting equilibrium mixtures. Such processes, having unprecedented separation factors coupled with the advantages of working in solution, could make enrichment of a large variety of isotopic species much more practical than is the case today.

We thank the NSF for support.

Note added in proof: the presence of sodium ions (even from the glass) can result in a decrease in the equilibrium constant for reaction (1) to well below unity.

Received 25 March; accepted 14 July 1986.

1. Tanaka, N., Yamaguchi, A. & Arki, M. *J. Am. chem. Soc.* 107, 7781–7782 (1985).
2. Stevenson, G. R., Espe, M. P. & Reiter, R. C. *J. Am. chem. Soc.* 108, 532–533 (1986).
3. Stevenson, G. R. & Hashim, R. T. *J. Am. chem. Soc.* 107, 5794–5795 (1985).
4. Lawler, R. D. & Fraenkel, G. K. *J. chem. Phys.* 49, 1126–1139 (1969).
5. Lawler, R. G. & Tabit, C. T. *J. Am. chem. Soc.* 91, 5671–5672 (1969).
6. Khatkale, M. S. & Devlin, J. P. *J. chem. Phys.* 70, 1851–1859 (1979).

Evaporative cooling of the western equatorial Pacific Ocean by anomalous winds

G. Meyers*, J. R. Donguy† & R. K. Reed‡

* CSIRO Division of Oceanography, Castray Espanade, Hobart, Tasmania 7000, Australia
† ORSTOM Groupe SURTROPAC, BP A5, Noumea, New Caledonia
‡ NOAA Pacific Marine Environmental Laboratory, Seattle, Washington 98115, USA

Global climate anomalies during El Niño/Southern Oscillation (ENSO) episodes are controlled by anomalous patterns of sea surface temperature (SST) in the equatorial Pacific Ocean[1–3]. Many studies during the past decade have indicated that warming of the eastern Pacific is caused by advection and downwelling associated with anomalous eastward currents[1–6]. Cooling of the western Pacific is probably not caused by an analogous process because zonal temperature gradients are small west of the dateline. We have searched for an explanation of the cooling because relatively small temperature changes in the west can be important in influencing the atmospheric general circulation[3,7,8]. Here we compare oceanic heat storage observed by expendable bathythermographs during 1979–83 with local processes in the heat budget, including various surface fluxes and mixing. The results show that cooling during 1982–83 was caused by evaporation due to anomalous meridional wind. The anomalous wind field in the region had been noted earlier by Harrison[9].

Ocean temperatures on meridional transects across the western Pacific between New Caledonia (or New Zealand) and Japan have been sampled since 1979 by volunteer observers on merchant ships, who take temperature soundings by XBT (expendable bathythermograph) to 450 m at 100-km intervals along the ship's track. The general transect is typically repeated once or twice a month. Details of the network have been given previously[10].

The surface temperature is coolest at the ends of the transect, where annual oscillation is the dominant variability (Fig. 1). The seasonal range is ~5–7 °C at higher latitudes. These oscillations are virtually extinguished within 10° of the Equator, where temperature usually exceeds 29 °C. During the first 3 years of our observations, this warm water mass was a stable feature. Then, beginning in June 1982, the warmest waters cooled by >1 °C, while the regular seasonal cooling at higher latitudes penetrated more deeply than normal into the tropics. This cooling episode persisted for 16 months, until the later part of 1983, when the 29 °C pool was re-established.

The monthly depth of the 26 °C isotherm (D_{26}) and the temperature (T_{26}) averaged vertically between the surface and D_{26} were used to characterize the heat content of the mixed layer in the 600-km band spanning the Equator from 2° S to 4° N. There were about 10 XBT stations in the area each month. Surface cooling during the 1982–83 ENSO episode is seen in T_{26}, with the most rapid cooling during the winter months of each hemisphere: July–August 1982 in the southern winter, then January–February 1983 in the northern winter (Fig. 2*a*). Shoaling of the thermocline by ~50 m during the 1982–83 ENSO episode as seen in D_{26} (Fig. 2*b*) will be discussed below.

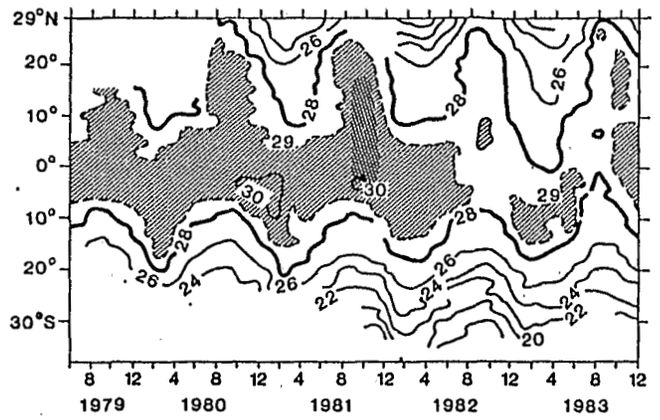

Fig. 1 Sea surface temperature on the shipping route between New Caledonia (or New Zealand) and Japan. Temperatures exceeding 29 °C are highlighted with single hatching. Double hatching indicates questionable values due to sparse data.

The processes that influence mixed-layer temperature are surface fluxes, horizontal advection by currents, entrainment mixing, turbulent diffusion, and penetrative radiation at D_{26} (refs 11, 12). The last two of these were found to be small in the equatorial Indian Ocean[11], and zonal advection is negligible. In the first model to be tested, the total surface flux (Q_T) is related to the change in upper-layer temperature by the relation

$$\rho C D_{26} \frac{\partial T_{26}}{\partial t} = Q_T \qquad (1)$$

where ρ and C are the density and heat capacity of water, and t is time. It is assumed in equation (1) that the mean surface flux is independently balanced by diffusion and advection, thus the equation applies only to fluctuations.

The local rate of heat storage, the left-hand side of equation (1), was calculated from T_{26} and D_{26}, and is typically of the order $\pm 40\ W\ m^{-2}$ (Fig. 2*f*). Periods of persistent cooling seen in T_{26} (Fig. 2*a*) are associated with the largest negative values of heat storage, as indicated by horizontal brackets. We seek an explanation for these cooling events.

The surface heat fluxes (insolation and net long-wave radiation, latent heat and sensible heat) on the right-hand side of equation (1) can be estimated from empirical formulae, using marine weather observations that include wind speed, SST, wet- and dry-bulb air temperature, and cloud cover. The formulae used in this study have recently been evaluated and are believed to be considerably more reliable than several earlier versions[13].

The individual marine weather observations, from ship-of-opportunity reports, were first converted to heat fluxes and then averaged monthly for the six 2°-latitude by 10°-longitude areas near the XBT observations (2° S–4° N, 150–170° E; Fig. 2*c–e*). The radiative fluxes (insolation minus net long-wave radiation; $Q_S - Q_B$) have a dominant semi-annual timescale recognized previously in other air/sea variables[14]. This signal is mainly due to the Sun's passing over the Equator twice a year. The turbulent fluxes (latent plus sensible heat; $Q_E + Q_H$) have a broader range of timescales, with persistent periods of high or low flux tending to last anywhere from a month to almost a year. The total flux Q_T, which is the difference between radiative and turbulent fluxes, is obviously dependent on the timescales and magnitudes of both ($Q_S - Q_B$) and ($Q_E + Q_H$).

A visual comparison of heat storage rate observed by XBT with total surface flux estimated from weather observations, suggests a correlation, particularly during 1982–83 (Fig. 2*e*, *f*). The cooling events of largest magnitude, indicated by horizontal bars, occurred during periods when the surface flux was below

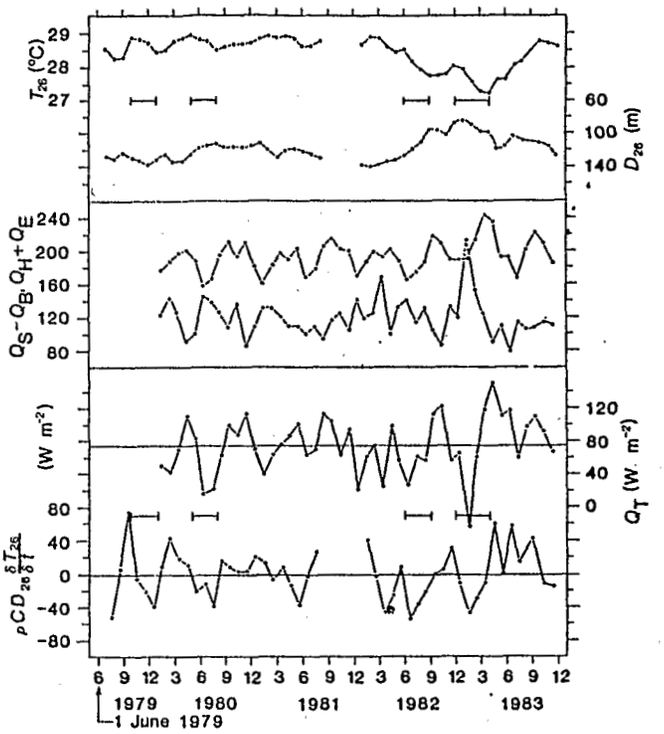

Fig. 2 *a*, Upper-layer temperature (T_{26}) averaged between the surface and the depth of the 26 °C isotherm (*b*, D_{26}). Heat fluxes at the sea surface: *c*, net radiation ($Q_S - Q_B$); *d*, net latent and sensible heat flux ($Q_E + Q_H$); *e*, total heat flux (Q_T), obtained by subtracting curve *d* from curve *c*; *f*, local heat storage rate ($\rho C D_{26} \partial T_{26}/\partial t$). Horizontal bars bracket times of largest cooling events.

the mean value ($75\ W\ m^{-2}$) for the 1979–83 period. The correlation coefficient is 0.45, which is significant at the 5% level, allowing for a decorrelation timescale of 2 months.

The next question is, which fluxes have the greatest effect on heat storage rates? Visual inspection of Fig. 2 suggests that changes are due more to irregular fluctuations in turbulent flux than to semi-annual oscillations in radiative flux. The correlations of the heat storage rate [$\rho C D_{26}(\partial T_{26}/\partial t)$] with each of the three heat flux terms (Q_T, $Q_E + Q_H$, and $Q_S - Q_B$) are 0.45, −0.46 and 0.23, respectively. More than 90% of the variance of $Q_E + Q_H$ is due to Q_E. Thus, latent flux is statistically most important, especially during 1982–83.

The weather variables used to calculate $Q_E + Q_H$ are wind speed (W), vertical gradient of vapour pressure ($e_s - e_a$), and vertical gradient of temperature ($T_s - T_a$), where the subscripts s and a indicate values at the sea surface and at 10 m height. The correlation coefficients of $Q_E + Q_H$ with W, $e_s - e_a$ and $T_s - T_a$ are 0.71, 0.26 and 0.47 respectively; they show wind as the dominant factor.

The coefficients given are correlations between turbulent flux and each atmospheric parameter individually. To take into account the relationships between atmospheric parameters, we used principal component analysis[15]. The three atmospheric parameters were first normalized by their standard deviations to make them dimensionless, and then the three normalized series were reduced to principal components. This produces three new time series, each one orthogonal to the other, and each a simple linear combination of W, $e_s - e_a$ and $T_s - T_a$. There is no *a priori* reason for any one principal component to be highly correlated to turbulent heat flux; however, one (Q_2) is.

In terms of the original data, Q_2 is calculated from the algebraic equation

$$Q_2 = 0.81\ W' + 0.58\ (T_s - T_a)' + 0.03\ (e_s - e_a)' \qquad (2)$$

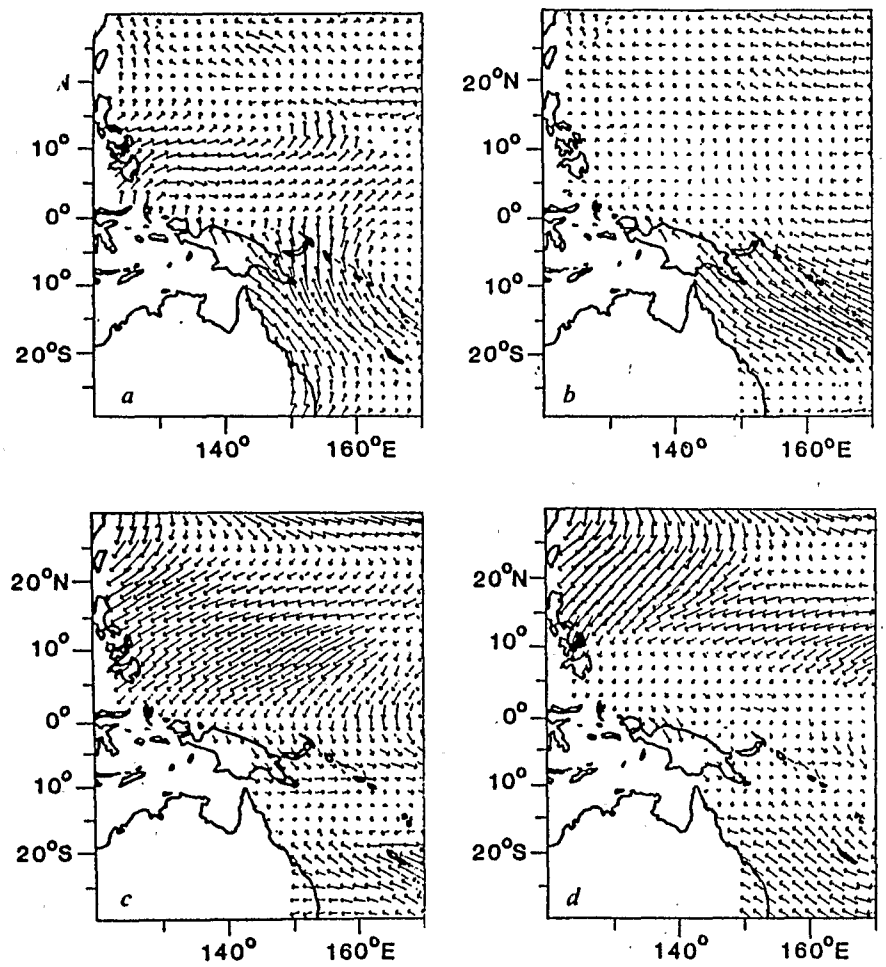

Fig. 3 The field of wind stress at the sea surface during two anomalous cooling periods in 1982–83 (*a*, July 1982; *c*, January 1983) and during two normal periods in 1981 (*b*, July 1981; *d*, January 1981).

where primes indicate that each parameter is measured relative to its mean value and normalized by its standard deviation. Remarkably, the correlation between $Q_E + Q_H$ and Q_2 is 0.89, which accounts for 79% of the turbulent flux variance. This is caused by the structure of Q_2, in which high wind speeds tend to occur at the same time as large $T_s - T_a$; such a situation increases turbulent flux. The structure of the first principal component (Q_1) had high wind speeds occurring at times of small $T_s - T_a$, producing opposite effects. Neither Q_1 nor the third principal component (Q_3) had a significant correlation with turbulent flux. The weight on W' in equation (2) again indicates that wind speed is the most important governing factor.

The weak dependence of Q_2 and $Q_E + Q_H$ on humidity ($e_s - e_a$) requires an explanation. Generally, humidity is not highly variable over the tropical ocean, as indicated statistically by its coefficient of variation (standard deviation divided by mean value), which is ~0.2. The coefficients of variation for W and $T_s - T_a$ are larger, of the order of unity.

The geographical structure of the cooling wind anomalies can be seen in atlases of Pacific trade-wind fields during recent years[16–18]. The wind field during July 1982 shows continuous meridional wind blowing from the Tasman Sea across the Equator (Fig. 3*a*). This wind does not penetrate so far equatorward during a normal year, such as 1981 (Fig. 3*b*), when winds near the Equator were weak and variable. The existence of the unusual wind field in 1982 and its effect on ocean currents have been examined by Harrison[9]. The meridional wind also affects the local surface heat budget, as discussed here. Another major cooling event in January 1983 (Fig. 3*c*) again shows a meridional wind blowing across the Equator, this time from the Northern Hemisphere. During a normal year, such as 1981, a weak and variable wind field is seen near the Equator (Fig. 3*d*). Cooling meridional wind coming from the winter hemisphere is probably a significant factor. Three additional cooling periods before June 1982 (Fig. 2*a*) are associated with strong wind from the winter hemisphere, as seen in the atlases[16–18]. These are September–December 1979, April–July 1980 and March–April 1982. Thus evaporative cooling at the Equator by anomalous meridional wind probably occurs on several timescales, ranging from brief, random weather inputs[19] to major El Niño episodes[20].

Entrainment is a cooling process in which cold water from the pycnocline is mixed into the surface layer. According to McPhaden[11], entrainment occurs only when the mixed layer deepens relative to an isotherm near the top of the thermocline. A test of entrainment in the western Pacific seemed necessary because D_{26} shoaled 50 m during the cooling episodes of 1982–83. Estimates of entrainment using McPhaden's method[11] for March–September 1982 and December 1982–April 1983 were, respectively, 4 W m^{-2} and 13 W m^{-2}. Thus, cooling by entrainment during the early stage of the episode (4 W m^{-2}) was negligible. Later, after the thermocline had shoaled by 50 m or more, its value (13 W m^{-2}) was still smaller than fluctuations in surface fluxes (20–40 W m^{-2}).

Evaporation by the wind has been shown here to be a probable cause of cool SST anomalies in the western equatorial Pacific. This observation identifies surface temperature change controlled by air/sea exchange of heat as part of ENSO. Earlier studies[1,2,4–6,21] have shown how oceanic heat is redistributed along the Equator, in an adiabatic process that does not involve air/sea heat exchange. This study suggests that the combined action of evaporative cooling west of the dateline and advective warming further east established the anomalous pattern of SST.

John Horel suggested a study of the role of western Pacific temperature in the Southern Oscillation. This research was supported by NSF grants during the Pacific Equatorial Ocean Dynamics (PEQUOD) programme, and by the Equatorial Pacific Ocean Climate Studies (EPOCS) programme of NOAA, and is contribution number 824 from the Pacific Marine Environmental Laboratory.

Received 6 May; accepted 17 July 1986.

1. Gill, A. E. & Rasmusson, E. M. *Nature* 306, 229–234 (1983).
2. Cane, M. G. *Science* 222, 1189–1194 (1983).
3. Nicholls, N. *Nature* 307, 576–577 (1983).
4. Wyrtki, K. *J. geophys. Res.* 90, 7129–7132 (1985).
5. Busalacchi, A. J., Takeuchi, K. & O'Brien, J. J. *J. geophys. Res.* 88, 7551–7562 (1983).
6. Harrison, D. E. & Schopf, P. S. *Mon. Weath. Rev.* 112, 923–933 (1984).
7. Palmer, T. N. & Mansfield, D. A. *Nature* 310, 483–485 (1985).
8. Simmons, A. J. *Q. J. R. met. Soc.* 108, 503–534 (1982).
9. Harrison, D. E. *Science* 224, 1099–1102 (1984).
10. Meyers, G. & Donguy, J. R. *Nature* 312, 258–260 (1984).
11. McPhaden, M. J. *J. mar. Res.* 40, 403–419 (1982).
12. Stevenson, J. W. & Niiler, P. P. *J. phys. Oceanogr.* 13, 1894–1907 (1983).
13. Reed, R. K. *J. geophys. Res.* 88, 9627–9638 (1983).
14. Meyers, G. *J. phys. Oceanogr.* 12, 1161–1168 (1982).
15. Lorenz, E. N. *Empirical Orthogonal Functions and Statistical Weather Prediction* (Science Rep. No. 1, Statistical Forcasting Project, MIT Department of Meteorology, Cambridge, 1956).
16. Legler, D. M. & O'Brien, J. J. *Atlas of Tropical Pacific Wind-Stress Climatology 1971–80* (Department of Meteorology, Florida State University, Tallahassee, 1984).
17. Leetma, A. & Wittee, J. (eds) *El Niño Atlas 1982–83* (Nova University Oceanographic Center Dania, 7L 33004, 1984).
18. Arkin, P. A., Kopman, J. D. & Reynolds, R. W. *1982–1983 El Niño/Southern Oscillation Event Quick Look Atlas* (NOAA National Weather Service, Washington DC, 1983).
19. Hasselmann, K. *Tellus* 28, 473–485 (1976).
20. Nicholls, H. *Mon. Weath. Rev.* 112, 424–432 (1984).
21. Philander, S. G. H. & Seigel, A. D. *Proc. 16th int. Liege Colloq. on Ocean Hydrodynamics* (ed. Nihoul, J.) (Elsevier, Amsterdam, 1985).

Coherent response of Arabian Sea upwelling and pollen transport to late Quaternary monsoonal winds

Warren L. Prell* & Elise Van Campo†

* Department of Geological Sciences, Brown University, Providence, Rhode Island 02912, USA
† Laboratoire de Palynologie, Université de Sciences et Techniques du Languedoc, 34060 Montpellier Cedex, France

The Indian summer monsoon causes large seasonal changes in the environments of both eastern Africa and the Arabian Sea. Here we compare time series (140 kyr long) of selected pollen types and foraminiferal upwelling faunas preserved in marine sediments, to identify the frequencies of their variability and the coherence and phase of the terrestrial and marine responses to monsoonal circulation. During interglacial intervals, the pollen and upwelling records of the western Arabian Sea indicate stronger monsoons and are both coherent and in phase at periodicities near the precession of the Earth's rotational axis (23 kyr). We conclude that the strength of the monsoonal southwesterlies accounts for this high coherence of marine and terrestrial records during interglacial intervals. Low correlation during glacial phases indicates weaker monsoons and some decoupling of these two records. These data indicate that two distinct modes of monsoon variability may exist: an interglacial mode with strong monsoons and effective coupling of terrestrial and marine records, and a glacial mode with both weaker monsoons and decreased linkage between Arabian Sea pollen and upwelling records.

The atmospheric circulation associated with the Indian summer monsoon reflects both the large-scale differential heating between Africa–Asia and the Indian Ocean, and the complex dynamics of the atmosphere–ocean system[1,2]. In the western Indian Ocean the summer monsoon circulation is characterized by cross-equatorial transport, strong low-level southwesterly winds (Fig. 1), coastal upwelling (Fig. 1), and increased precipitation[1–5]. Changes in these climatic variables have been inferred from a large variety of geological data, including palaeolake levels[6,7], pollen spectra[8,9], wind-transported materials[10], and distribution of planktonic faunas[11–13]. These studies indicate that the monsoon was weaker ~18,000 yr ago, during maximum glacial conditions[14–17], and stronger ~9,000 yr ago, when the Northern Hemisphere received ~7% more summer insolation than at present[4–7,11,17,18]. Although the monsoonal circulation affects both continents and oceans, relatively few studies have compared the responses of these two environments. However, some studies have been able to document the abundance of terrestrial components, such as pollen[8,9,17], fresh-water diatoms[10] and phytoliths[10] in marine sediments, and thereby take advantage of the continuous and well-dated nature of marine records. In the western Arabian Sea, records of monsoonal upwelling faunas and wind-transported pollen are preserved in the deep-sea sediments. Our objective here is to determine the coherence of these marine and terrestrial data and to establish their relative response to long-term changes in seasonal solar radiation and glacial boundary conditions (that is, changes of the volume and extent of ice sheets, surface albedo and sea surface temperatures).

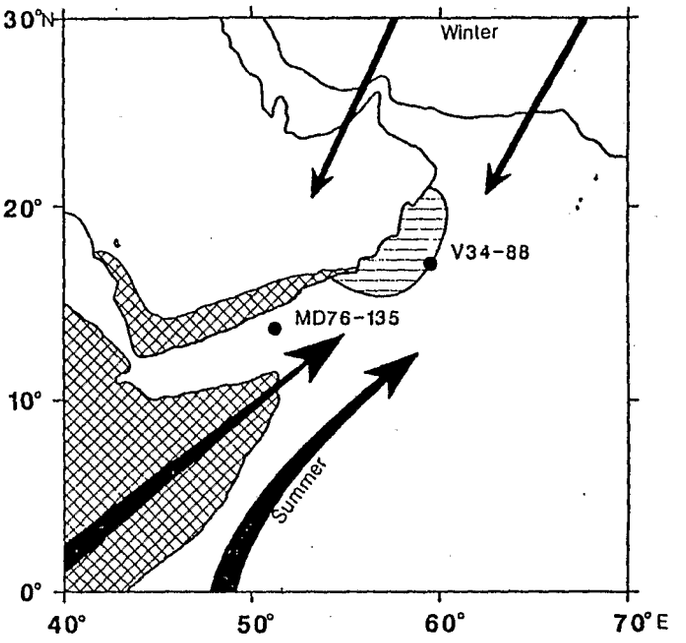

Fig. 1 Location of cores MD76-135 (containing the monsoon pollen index, MPI) and V34-88 (containing the monsoon upwelling index, MUI). The generalized source area for the MPI[26,27] is indicated by the cross-hatched pattern, and the area of maximum upwelling and MUI[11,12,23–25] is shown by horizontal shading. Arrows indicate the direction and relative strength of summer southwesterly and winter northeasterly winds.

We used graphic correlation of oxygen isotopic events[19–21] to correlate two Arabian Sea cores that contain indices of monsoonal intensity (Fig. 1). Core MD76-135 (14°27′ N, 50°31′ E; 1,895 m water depth) has an isotopic stratigraphy measured by J. C. Duplessy[16]; that of core V34-88 (16° N, 60° E; 2,800 m) was measured by Prell[22]. The correlation of isotopic stratigraphy between the two cores is good, considering their different accumulation rates (V34-88, 4 cm kyr^{-1}; MD76-135, 8–12 cm kyr^{-1}), the different species used for the isotopic measurements (Fig. 2), and their different depositional environments. The isotopic events were used with the SPECMAP age